NGC 300 X–1 is a Wolf-Rayet/Black-Hole binary*

P. A. Crowther[1]†, R. Barnard[2], S. Carpano[3], J. S. Clark[2], V. S. Dhillon[1], A. M. T. Pollock[3]

[1] *Department of Physics and Astronomy, University of Sheffield, Sheffield S3 7RH, UK*
[2] *Department of Physics and Astronomy, The Open University, Walton Hall, Milton Keynes, MK7 6AA, UK*
[3] *XMM-Newton Science Operations Center, ESAC, 28080, Madrid, Spain*

6 January 2010

ABSTRACT

We present VLT/FORS2 time-series spectroscopy of the Wolf-Rayet star #41 in the Sculptor group galaxy NGC 300. We confirm a physical association with NGC 300 X–1, since radial velocity variations of the He II λ4686 line indicate an orbital period of 32.3 ± 0.2 hr which agrees at the 2σ level with the X-ray period from Carpano et al. We measure a radial velocity semi-amplitude of 267 ± 8 km s^{-1}, from which a mass function of 2.6 ± 0.3 $M_\odot$ is obtained. A revised spectroscopic mass for the WN-type companion of 26^{+7}_{-5} $M_\odot$ yields a black hole mass of 20 ± 4 $M_\odot$ for a preferred inclination of $60 - 75°$. If the WR star provides half of the measured visual continuum flux, a reduced WR (black hole) mass of $15^{+4}_{-2.5}$ $M_\odot$ ($14.5^{+3}_{-2.5}$ $M_\odot$) would be inferred. As such, #41/NGC 300 X–1 represents only the second extragalactic Wolf-Rayet plus black-hole binary system, after IC 10 X–1. In addition, the compact object responsible for NGC 300 X–1 is the second highest stellar-mass black hole known to date, exceeded only by IC 10 X–1.

Key words: (galaxies:) individual: NGC 300 – Stars: Wolf-Rayet – X-rays: binaries – X-rays: individual: NGC 300 X–1

1 INTRODUCTION

High mass X-ray binaries (HMXB) typically comprise OB stars plus either a neutron star or black hole, in which high X-ray luminosities ($\sim 10^{38}$ erg s^{-1}) arise from accretion disks around the compact object. Accretion disks are fed through a combination of Roche lobe overflow and stellar winds from the early-type companion. Very few known HMXB are known to host black-holes, Cyg X–1 in the Milky Way, X–1 and X–3 in the Large Magellanic Cloud and X–7 in the Local Group galaxy M 33. If a merger is avoided, the OB companion will potentially evolve through to a Wolf-Rayet phase, producing a system comprising a helium star plus a black hole or neutron star (Tutukov & Yungelson 1973). Indeed, van den Heuvel & de Loore (1973) proposed the Galactic HMXB Cyg X–3 as a helium-star plus compact object system, which was observationally confirmed by van Kerkwijk et al. (1992). Such systems are believed to be very rare, with as few as ~ 100 helium star plus black hole pairs in the Galaxy (Ergma & Yungelson 1998).

To date, the only confirmed Wolf-Rayet plus black hole binary system is IC 10 X–1 in the dwarf irregular galaxy IC 10. This system has a period of 34.9 hr, hosts a WN-type Wolf-Rayet star [MAC 92] 17A (Crowther et al. 2003) and an unseen companion which is currently the record holder amongst stellar mass black

Table 1. Log of VLT/FORS2 spectroscopic observations of #41 in NGC 300. UT dates and MJD's refer to the start of the 1,535 s exposures. We include centroid of gaussian fits to He II λ4686 lines, λ_{4686}. Phases adopt a period of 32.3 hr, where phase 0 refers to MJD 55118.97559±0.01554).

UT Date	MJD −55119	DIMM ''	sec z	v_r λ4686 km s^{-1}	Phase
01:06 15 Oct 09	0.046180	1.2	1.29	347.0 ± 17.7	0.052
05:28 15 Oct 09	0.227922	2.3	1.08	364.6 ± 25.5	0.187
01:40 16 Oct 09	1.069495	1.1	1.18	−64.2 ± 16.9	0.812
05:58 16 Oct 09	1.249073	1.7	1.14	136.0 ± 25.0	0.945
04:07 19 Oct 09	4.171590	0.7	1.03	369.0 ± 14.3	0.114
08:24 19 Oct 09	4.350382	0.8	1.98	456.6 ± 20.1	0.247
02:31 20 Oct 09	5.104896	0.9	1.06	−68.3 ± 12.1	0.807
06:41 20 Oct 09	5.278856	0.7	1.31	109.4 ± 17.3	0.936
00:14 25 Oct 09	10.010318	1.2	1.34	325.3 ± 25.7	0.447
06:28 25 Oct 09	10.269520	0.7	1.33	10.4 ± 14.3	0.639

holes, exceeding 23.1±2.1 $M_\odot$ (Prestwich et al. 2007; Silverman & Filippenko 2008).

A second candidate extragalactic black hole plus Wolf-Rayet system is NGC 300 X–1 (Carpano et al. 2007a), in the southern Sculptor group spiral galaxy NGC 300 which lies at a distance of 1.88 Mpc (Gieren et al. 2005). This source is spatially coincident with #41 from the Wolf-Rayet catalogue of Schild et al. (2003)
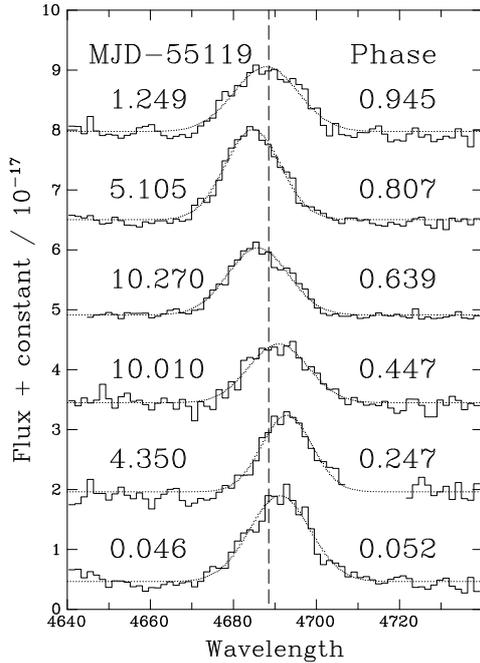
Figure 1. Representative VLT/FORS2 spectroscopy of #41 revealing radial velocity variations in He II $\lambda 4686$ (gaussian fits are shown as dotted lines), successively offset by 1.5×10^{-17} erg s^{-1} cm^{-2} Å^{-1} for clarity.

which was confirmed as a WN-type Wolf-Rayet star by Crowther et al. (2007). Both systems exhibit similar X-ray properties (Carpano et al. 2007b; Barnard, Clark & Kolb 2008). However, no evidence exists to date of a physical link between NGC 300 X–1 and the Wolf-Rayet star #41. This is the purpose of the present Letter.

New Very Large Telescope (VLT) optical spectroscopic time-series of #41 are discussed in § 2 in which variations are revealed in the He II $\lambda 4686$ emission line. § 3 compares the inferred orbital period with X-ray lightcurves and derives a semi-amplitude for the Wolf-Rayet star, from which a mass function is obtained. § 4 provides a revised mass for the Wolf-Rayet star, placing strict limits upon the mass of the compact companion. We conclude with a brief discussion in § 5.

2 OBSERVATIONS

Here we present new VLT optical spectroscopy of #41 obtained with the Focal Reducer/Low Dispersion Spectrograph #2 (FORS2) in multi-object spectroscopy (MOS) mode from 14–24 October 2009. Two 1,535 s exposures were obtained on each of five non-consecutive nights using the 600B grism, centred at 465 nm. A log of our observations is presented in Table 1 including DIMM seeing measurements, which indicated typical seeing of 0.7–1.2 arcsec, except at two epochs for which the seeing exceeded 1.5 arcsec.

MOS allows 19 sources to be simultaneously observed. We included 7 H II regions in NGC 300 plus 12 WR candidates from Schild et al. (2003). Of these, 3 sources have previously been spectroscopically confirmed as WR stars, namely #9, #41 and source 12 from Bresolin et al. (2009). Other sources will be discussed elsewhere.

After bias subtraction and flat field correction, a standard extraction was performed using IRAF, with wavelength and flux calibration carried out using FIGARO. 1.0 arcsec slits provided a spec-
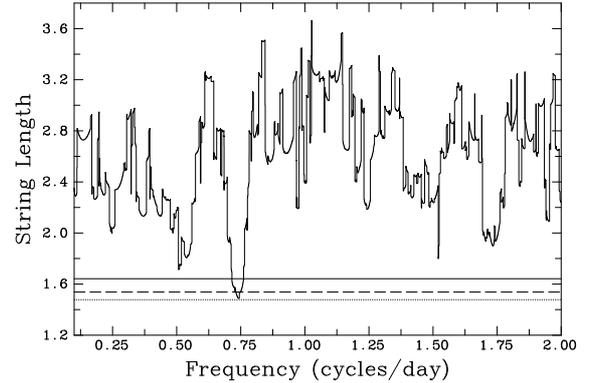
Figure 2. String-length periodogram of the VLT/FORS2 radial velocities. The minimum string length indicates the best period, at a frequency of 0.7422 cycles/day. The solid, dashed and dotted lines represent the 68.3%, 95.4% and 99.7% confidence levels, respectively (see text for details).

tral resolution of 4.2 Å – as measured from comparison arc lines – with a wavelength coverage of 3300–5800Å for #41. Faint Hβ and [O III] $\lambda 4959$, 5007 nebular lines were detected in the #41 slit. #41 does not appear to be responsible for these features since the intensity of the nebula is weak and spatially close to #41, and has a lower systemic velocity of $\sim$95 km s^{-1} (versus 202 km s^{-1} for #41).

Spectrophotometric standard stars were observed with FORS2 in long slit mode on the nights on 15 Oct (HD 49798), 18–19 Oct (LTT 2415) and 24 Oct (LTT 7987), providing a wavelength coverage of 3300-6230Å. An absolute flux calibration was achieved for #41 using B = 22.71 mag from Carpano (2006).

3 ORBITAL PERIOD

Several VLT/FORS2 spectroscopic observations in the vicinity of He II $\lambda 4686$ are presented in Fig. 1, revealing large radial velocity variations. Gaussian profiles are fit to individual $\lambda 4686$ profiles, with individual centroids listed in Table 1.

In view of the sparsely sampled datasets, we have employed the string-length approach of Dworetsky (1983). The data are folded on a set of trial frequencies and the total length of "string" required to join the observations in phase order is calculated. The smallest string length found from the search is assumed to correspond to the correct period. The resulting periodogram is shown in Fig. 2. The deepest trough corresponds to a period of 32.3 ± 0.2 hr. The error on this period was computed by constructing 10 000 synthesized datasets and measuring the standard deviation of the positions of the deepest troughs in the resulting periodograms. The synthesized datasets were obtained by "jiggling" each data point about its observed value by an amount given by its error bar multiplied by a number output by a Gaussian random-number generator with zero mean and unit variance.

It can be seen that our derived period is in agreement at the 2σ level with the Swift X-ray period of 32.8 ± 0.2 hr (1σ; Carpano et al. 2007b), which gives us confidence that we have identified the correct value. Moreover, the minimum string length of our period (1.49) compares favourably with the string length of a perfect sinusoid (1.46) and the string length of a sinusoid with noise consistent with the error bars on the observed data added to it (1.48).

To further test the significance of our derived period, we used a randomization technique (Fisher 1935). The radial velocities were

randomly reassigned to the times of observation, thereby preserving the data sampling and the mean and standard deviation of the original dataset. A set of 10 000 randomised datasets were constructed in this way and then subjected to the same string-length periodogram analysis. By constructing a cumulative distribution function of the resulting minimum string lengths, we are able to place confidence limits on the significance of a given string length, as shown by the horizontal lines in Fig. 2. We are able to reject the hypothesis that our preferred period is due to noise at 99.43% confidence and eliminate the next highest troughs as most likely due to noise. Note that the troughs around 0.25 and 1.75 cycles/day are due to the one-cycle-per-day alias. As a check on the string length method, we also computed a Lomb-Scargle periodogram (Press & Rybicki 1989) and obtained consistent results.

Adopting our optical period, we present the phased radial velocity measurements in Fig. 3, with a semi-amplitude of $K_2 = 267.5 \pm 7.7$ km s^{-1}. In the Figure, phase 0 corresponds to MJD 55118.97559 ± 0.01554.

Armed with the semi-amplitude and orbital period, we may now derive the system mass function,

$$f(m) = \frac{PK_2^3}{2\pi G} = \frac{M_1 \sin^3 i}{(1+q)^2}$$

where M_1 is the compact object mass, and $q = M_2/M_1$. The derived mass function is $f(m) = 2.63 \pm 0.33\,M_\odot$, and would correspond to the compact object mass in the case of a system viewed at an inclination of $90°$ whose companion mass is negligible. In the case of a massive companion star with $q \sim 1$, the compact object would have a minimum mass of 4 $f(m)$. As such, the compact object in NGC 300 X–1 is indeed a black hole, such that this system represents only the second confirmed WR plus black hole binary.

4 WOLF-RAYET PROPERTIES

We present our new, combined (phase-corrected), rectified VLT/FORS2 spectrum of #41 in Fig. 4. This high quality spectrum confirms a weak-lined WN5 subtype, previously inferred by Crowther et al. (2007) from lower resolution, lower S/N spectroscopy obtained with VLT/FORS2 using the 300V grism in January 2007. Overall, the visual spectrum of #41 is similar to other weak-lined WN5 stars, namely WR 49 in the Milky Way and Brey 65b (= NGC 2044 West 5C) in the LMC, taken from Hamann et al. (1995) and Walborn et al. (1999), respectively. The He II $\lambda 4686$ equivalent width ($W_\lambda \sim 56$Å), and line width (FWHM~ 17Å) in #41 are somewhat lower than LMC and Milky Way counterparts, $W_\lambda = 110$–140Å and FWHM=22–24Å.

In order to reassess the mass of #41 we have calculated a synthetic model using the Hillier & Miller (1998) line-blanketed, non-LTE model atmosphere code. With respect to Crowther et al. (2007), somewhat more sophisticated atomic models are considered, namely H, He, C, N, O, Ne, Si, P, S, Ar, Fe and Ni. Elemental abundances are set to 40% of the solar value (Urbaneja et al. 2005), with the exception of H and CNO elements. Clumping is accounted for, albeit in an approximate manner, with a (maximum) volume filling factor of 10%, such that the derived mass-loss rate is three times smaller than the value that would have been obtained by assuming an homogeneous wind.

In view of the weak He I line spectrum in #41, we have based our analysis upon He II ($\lambda 4686$, $\lambda 5411$) and N IV-V ($\lambda\lambda 4603$–20, $\lambda 4058$, $\lambda 7103$–7129) line diagnostics. Overall good agreement is found, which is remarkable in view of the close proximity of the
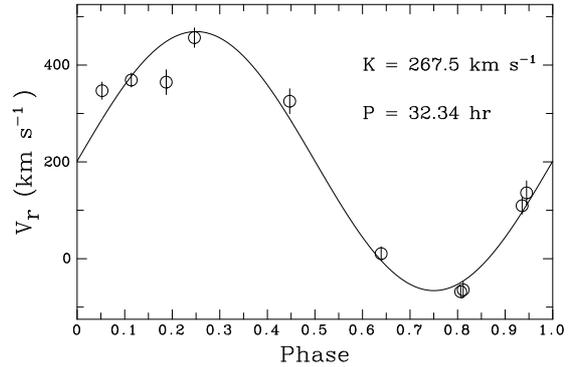
Figure 3. Radial velocity variations of $\lambda 4686$ He II phased to 32.3 hr, from which a systemic velocity of $v_r = 202 \pm 7$ km s^{-1} and semi-amplitude of $K_2 = 267.5 \pm 7.7$ km s^{-1} is obtained.
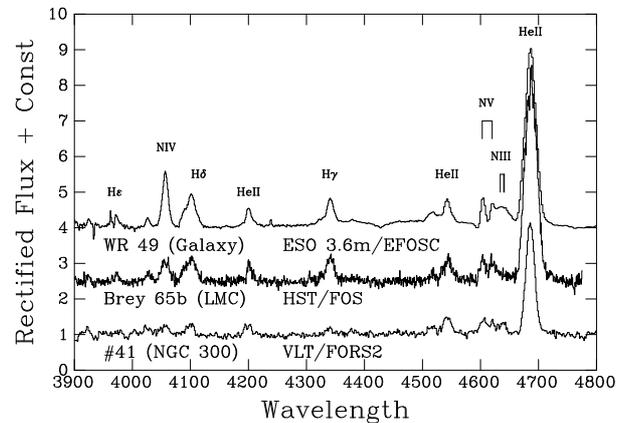
Figure 4. Comparison between rectified, phase corrected VLT/FORS2 spectrum of #41 with Galactic (WR 49) and LMC (Brey 65b = NGC 2044 West 5C) weak-lined WN5 stars, respectively from Hamann et al. (1995) and Walborn et al. (1999).

black hole to #41. The only significant discrepancies are that N III $\lambda 4634$–41 is not reproduced in the synthetic spectrum and excess emission is observed in the upper Pickering-Balmer series, the latter potentially arising from the accretion disk.

In Fig. 5 we present our new combined flux calibrated spectrum of #41, together with re-calibrated spectroscopy from Crowther et al. (2007) for $\lambda > 5800$Å. An optimum fit to the spectrum of #41 is included in the figure, and reveals the following stellar parameters – $T_* \sim 65$ kK, $\log(L/L_\odot) \sim 5.92$, $\dot{M} \approx 5 \times 10^{-6}$ M$_\odot$ yr^{-1}, $v_\infty \sim 1300$ km s^{-1}, plus a nitrogen mass fraction of ~ 0.5%, with negligible hydrogen adopted. With respect to Crowther et al. (2007), the main revision relates to a reduced absolute magnitude of $M_V = -5.0$ mag, on the basis of a lower interstellar reddening of $E(B-V) = 0.4$ mag. T_* should be reliable to ± 5 kK, resulting in uncertainties of ± 0.2 mag in bolometric corrections. Together with ± 0.05 mag uncertainties in $E(B-V)$, stellar luminosities should be reliable to ± 0.14 dex.

From our derived parameters, we obtain a spectroscopic WR mass of 26^{+7}_{-5} M$_\odot$ on the basis of the Schaerer & Maeder (1992) mass-luminosity relation for hydrogen-free WR stars. The principal uncertainty in our inferred WR mass relates to the absolute visual magnitude of the WR star. Since our adopted visual magnitude is

Figure 5. Combined, phase-corrected VLT/FORS2 spectroscopy of #41 from Oct 2009 and Jan 2007 (black) with synthetic spectrum overlaid (red), reddened by $E(B-V)$=0.4 mag, as described in § 4.

Table 2. Derived black hole mass, M_1, in NGC 300 X–1 for i=45, 60° or 90°, for cases in which the WN star contributes either 50% ($M_2 = 15M_\odot$) or 100% ($M_2 = 26M_\odot$) of the visual light. We include the separation between the components, a, and the WR radius, R_2, as a fraction of the Roche lobe radius, r_L (Eggleton 1983).

M_2 (WR) $M_\odot$	R_2 (WR) $R_\odot$	i	M_1 (BH) $M_\odot$	a $R_\odot$	R_2/r_L
$15^{+4}_{-2.5}$	4.8 ± 0.1	45^1	$21.5^{+2.5}_{-1.7}$	$17.0^{+0.9}_{-0.7}$	0.81
$15^{+4}_{-2.5}$	4.8 ± 0.1	60	$15.6^{+1.9}_{-1.4}$	$16.1^{+1.0}_{-0.7}$	0.80
$15^{+4}_{-2.5}$	4.8 ± 0.1	90^1	$12.6^{+1.6}_{-1.3}$	$15.5^{+1.0}_{-0.8}$	0.79
26^{+7}_{-5}	7.2 ± 0.1	45^1	$27.8^{+3.5}_{-2.8}$	$19.4^{+1.2}_{-1.0}$	0.99
26^{+7}_{-5}	7.2 ± 0.1	60	$20.6^{+2.9}_{-2.1}$	$18.5^{+1.3}_{-1.0}$	0.98
26^{+7}_{-5}	7.2 ± 0.1	90^1	$16.9^{+2.4}_{-1.9}$	$18.0^{+1.2}_{-1.0}$	0.96

[1] The apparent glancing eclipse of the X-ray emitting accretion disk suggests $i = 60 - 75°$.

ponents using Kepler's third law in each case, obtained from

$$P = \frac{2\pi a^{3/2}}{[G(M_1 + M_2)]^{1/2}},$$

corresponding to only 2.5–3.5 Wolf-Rayet radii. The mass accretion rate required to sustain $L_X = 2 \times 10^{38}$ erg s^{-1} is 3.5 $\times 10^{-8} M_\odot$ yr^{-1}, if the adopted efficiency of gravitational release is ~10% (see Shakura & Sunyaev 1973). This is ≤ 1% of our derived mass-loss rate of #41. However, Table 2 also shows that the WR star would completely fill its Roche lobe for the 26 $M_\odot$ case ($i \leq 35°$ is excluded), and equates to 80% of its Roche lobe radius, r_L (Eggleton 1983), for the 15 $M_\odot$ case. Therefore, the accretion disk may be fed primarily through Roche lobe overflow. For comparison, the higher temperature obtained for the WN star in IC 10 X–1 by Clark & Crowther (2004) would favour a wind-fed accretion disk, since the WR radius is $\sim 0.5r_L$ in that system.

IC 10 X–1 is an eclipsing X-ray system (Prestwich et al. 2007), therefore geometric arguments imply that the black hole would be eclipsed for $i \geq 78°$ for the WR properties derived by Clark & Crowther (2004). If we adopt a radius of $\sim 0.5r_L$ for the accretion disk, an eclipse of the X-ray emitting accretion disk would require $i \geq 80°$. NGC 300 X–1 does exhibit significant X-ray variability, but lacks a deep X-ray eclipse (Carpano et al. 2007b). Therefore, geometric arguments appear to rule out inclinations that would cause a total eclipse of the accretion disk ($i \leq 73 \pm 2°$). However, a glancing eclipse would require $i \geq 63.5 \pm 3.5°$ for the range of WR radii obtained here. We therefore adopt $i = 80 - 90°$ for IC 10 X–1 and $i = 60 - 75°$ for NGC 300 X–1.

In Fig. 6 we present the host galaxy metallicity as a function of black hole masses for NGC 300 X–1 and IC 10 X–1, plus those for all HMXB systems for which the presence of a black hole is unambiguous, whose companion is an OB star with mass $M_2 \geq 5M_\odot$, i.e. LMC X–3 (Val-Baker et al. 2007), LMC X–1 (Orosz, Steeghs & McClintock 2009), M33 X–7 (Orosz et al. 2007), V4641 Sgr (Orosz et al. 2001) and Cyg X–1 (Gies et al. 2003). We limit our sample to classical HMXB, to ensure that their present-day (oxygen) metallicities are consistent with the formation of these black hole binaries. The majority of black holes in Low Mass X-ray Binary (LMXB) systems have masses close to $10M_\odot$ (Remillard & McClintock 2006).

It may be significant that both Wolf-Rayet/black hole systems are located in metal-poor galaxies. IC 10 has an oxygen content

based upon ground-based imaging, it is possible that other continuum sources are included in the photometry. In this case, the WR emission line equivalent width would be diluted by the continuum of other nearby sources.

Indeed, while #41 closely resembles other weak-lined WN5 stars (recall Fig. 4), its He II $\lambda4686$ equivalent width is indeed lower by a factor of ~2. This hints at a potential factor of two line dilution from unresolved companions along the sight-line towards #41. In this case, the WR luminosity would be reduced to $\log(L/L_\odot)$ = 5.57$\pm$0.14 with the mass-loss rate unaffected, implying a spectroscopic mass of $15^{+4}_{-2.5}M_\odot$. For reference, Hamann, Gräfener, & Liermann (2006) estimated spectroscopic masses of 15–19 $M_\odot$ for weak-lined WN5 stars in the Milky Way. In view of these issues, we shall evaluate black hole masses using values of both 15 and 26 $M_\odot$ for the WN star.

5   DISCUSSION AND CONCLUSIONS

In Table 2 we present black hole masses for inclinations of 45, 60 and 90° for our favoured 26 $M_\odot$ spectroscopic WR mass, plus the 15 $M_\odot$ case, resulting from the WR star contributing 50% of the visual continuum light. We include the separation between the com-

Figure 6. Comparison between inferred compact object masses, M_1, versus metallicity for all HMXB with $M_1 \geq 3M_\odot$ and $M_2 \geq 5M_\odot$. Black hole masses inferred for NGC 300 X–1 (IC 10 X–1) relate to a WR mass of 21^{+5}_{-6} $M_\odot$ (25^{+13}_{-8} $M_\odot$) and an orbital inclination of 60–75° (80–90°).

of log (O/H) + 12 = 8.1 (Garnett 1990) while NGC 300 X–1/#41 is located at a de-projected distance of 0.43 ρ_0, where ρ_0 = 9.75 arcmin (Schild et al. 2003). According to Urbaneja et al. (2005), the oxygen content at this galactocentric distance in NGC 300 is log (O/H) + 12 ∼ 8.44, i.e. relatively similar to the LMC for which log (O/H) + 12 ∼ 8.37 (Russell & Dopita 1993). The only other HMXB whose black hole mass is known to greatly exceed 10 $M_\odot$ is M 33 X–7 (Orosz et al. 2007), for which a near identical oxygen content of log (O/H) + 12 = 8.42 is inferred at its location in M 33 from the calibration of Magrini et al. (2007).

High black hole masses require that the progenitor star was very massive and experienced low mass-loss rates (Belczynski et al. 2009). Weak stellar winds is a natural consequence of low metallicity (Mokiem et al. 2007). However, orbital periods of IC 10 X–1 and NGC 300 X–1 are so short that the radius of the black hole progenitor star must have been larger than the present separation of the components. As such, the progenitor would have experienced extreme mass-loss through Roche-lobe overflow. Therefore, reconciling high black hole masses with close orbital separations is a major challenge for binary evolution models.

In the standard picture, such systems involve a common-envelope phase, which would naturally lead to a merger (Podsiadlowski, Rappaport & Han 2003). Alternatively, de Mink et al. (2009) propose that the short orbital period results in tidal-locking of the stellar rotation, causing a chemically homogeneous evolution through rotational mixing (Maeder 1987). In this scenario, binary components would remain compact and so circumvent the high mass transfer rates of Roche-lobe overflow systems.

If NGC 300 X–1 and IC 10 X–1 were to survive their second supernova explosion, they would form binary black hole systems, merging on a timescale of a few Gyr. Binary black hole mergers has been considered by Sadowski et al. (2008), who argued that their detection rate may be much higher than double neutron star systems for current gravitational wave experiments.

In conclusion, new VLT/FORS2 time-series spectroscopy of the WN star #41 in NGC 300 is presented, which confirm that it is physically associated with the NGC 300 X–1 system. We find that NGC 300 X–1 hosts the most massive stellar-mass black hole known, with the exception of the other extragalactic WR/black hole system IC 10 X–1.

REFERENCES

Barnard, R., Clark, J.S., Kolb, U.C., 2008, A&A 488, 697
Belczynski, K., Bulik, T., Fryer, C.L., Ruiter, A., Vink, J.S., Hurley, J.R. 2009, ApJ submitted (arXiv:0904.2784)
Bresolin F., Gieren, W., Kudritzki, R.-P. et al. 2009, ApJ 700, 309
Carpano S., 2006, PhD Thesis, Universität Tübingen, Germany
Carpano S., Pollock A.M.T., Wilms J., Ehle M., Schirmer M., 2007a, A&A 461, L9
Carpano S., Pollock A.M.T., Prestwich A., et al. 2007b, A&A 466, L17
Clark, J.S., Crowther, P.A., 2004, A&A 414, L45
Crowther P.A., Drissen L., Abbott J.B., Royer P., Smartt S.J. 2003, A&A 404, 483
Crowther, P.A., Carpano, S., Hadfield, L.J., Pollock, A.M.T. 2007, A&A 469, L31
de Mink, S.E., Cantiello, M., Langer, N. et al. 2009, A&A 497, 243
Dworetsky, M.M., 1983, MNRAS 203, 917
Eggleton, P.P., 1983, ApJ 268, 368
Ergma E., Yungelson L.R. 1998, A&A 33, 151
Fisher, R.A., 1935, The Design of Experiments. New York: Hafner
Garnett, D. 1990, ApJ 363, 142
Gieren W., Pietrzynski G., Soszynski I. et al. 2005, ApJ 628, 695
Gies, D.R., Bolton, C.T., Thomson, J.R. et al. 2003, ApJ 583, 424
Hamann, W.-R., Koesterke, L., Wessolowski, U., 1995, A&AS 113, 459
Hamann, W.-R., Gräfener, G., Liermann, A., 2006, A&A 457, 1015
Hillier D.J., Miller D.L., 1998, ApJ 496, 407
Maeder, A., 1987, A&A 178, 159
Magrini, L., Vilchez, J.M., Mampaso, A. et al. 2007, A&A 470, 865
Mokiem, M.R., de Koter A., Vink J.S. et al. 2007, A&A 473, 603
Orosz, J.A., Kuulkers, E., van der Kils, M. et al. 2001, ApJ 555, 489
Orosz, J.A., McClintock J.E., Narayan, R. et al. 2007, Nat 449, 872
Orosz, J.A., Steeghs, D., McClintock, J.E. 2009, ApJ 697, 573
Podsiadlowski, P., Rappaport, S., Han, Z., 2003, MNRAS, 341, 385
Press, W.H., Rybicki, G.B., 1989, ApJ 338, 277
Prestwich A.H., Kilgard R., Crowther P.A. et al. 2007, ApJ, 669, L21
Remillard, R.A., McClintock, J.E. 2006, ARA&A 44, 49
Russell, S.C., Dopita, M.A., 1990, ApJS 74, 93
Sadowski, A., Belczynski, K., Bulik, T., Ivanova, N., Rasio, F.R., O'Shaughnessy, R. 2008, ApJ 676, 1162
Schaerer D., Maeder A. 1992, A&A 263, 129
Schild H., Crowther P.A., Abbott J.B., Schmutz W. 2003, A&A 397, 859
Shakura, N.I., Sunyaev, R.A., 1973, A&A 24, 337
Silverman, J.M., Filippenko, A.V. 2008, ApJ, 678, L17
Tutukov, A., Yungelson, L., 1973, Nauchnye Informatsii, 27, 70
Urbaneja, M.A., Herrero, A., Kudritzki, R.-P. et al. 2005, ApJ 622, 862
Val-Baker, A.K.F., Norton, A.J., Negueruela, I., 2007, in: The Multi-coloured Landscape of Compact Objects and their Explosive Origins, Di Salvo, T., et al. (eds), AIP 924, 530
van den Heuvel, E.P.J., de Loore, C., 1973. A&A 25, 387
van Kerkwijk, M.H., Charles, P.A., Geballe, T.R. et al. 1992, Nat 355, 703
Walborn, N.R., Drissen, L., Parker, J.W. et al. 1999, AJ 118, 1684